

Signature of collective effects in the frequency-comb-induced radiation pressure force

M. Kruljac,¹ D. Buhin,¹ D. Kovačić,¹ V. Vulić,¹ D. Aumiler,¹ and T. Ban¹

¹*Institute of Physics, Bijenička cesta 46, 10000 Zagreb, Croatia*

(Dated: February 19, 2021)

We investigate the modifications of the frequency-comb-induced radiation pressure force on cold ^{87}Rb atoms that are induced by the collective effects. Collective effects include both coherent and incoherent contributions and depend on the optical thickness of the atomic cloud. We observe reduction and broadening of the comb-induced force when the cloud's optical thickness increases, and compare the measured results with predictions of a coherent model based on the timed Dicke state approach and an incoherent scattering model based on the shadow effect explained by Beer-Lambert law. Both models describe the experimental results well, indicating that an incoherent scattering approach is sufficient to explain the observed modifications of the comb-induced force even for larger optical thicknesses. The results support the analogy between the frequency comb and continuous-wave laser-atom interaction and thus pave the way toward novel frequency comb applications in laser cooling, quantum communication, and light-atom interfaces based on structured and disordered atomic systems.

PACS numbers: 37.10.De, 37.10.Vz

I. INTRODUCTION

Optical frequency combs (FCs) have become an unavoidable source of light in applications ranging from metrology [1, 2] and high-resolution spectroscopy [3–5] to precision ranging [6] and calibration of atomic spectrographs [7]. In recent years, the applications of FCs have expanded to laser cooling and trapping of atoms and ions, and quantum communication. Recent demonstrations include FC cooling of ions [8, 9], neutral atoms [10, 11], and simultaneous dual-species FC cooling [12]. Applications of the FC for quantum communication are based on the recent progress in generating highly multimode nonclassical FCs [13–16] and the potential for the realization of multi-mode quantum memories [17, 18]. For these novel and intriguing applications of FCs that are at the core of quantum technologies, it is necessary to understand the FC light-matter interactions, and to verify whether and to what extent these interactions are comparable to already known continuous-wave (cw) laser-matter interactions. In this respect, it is particularly important to understand FC light scattering and all effects that accompany it.

Collective effects observed in light scattered from an ensemble of cold atoms illuminated by a cw laser have been an extremely fruitful platform for studying light-matter interactions [19–23]. The light scattered by the atomic ensemble contains coherent and incoherent contributions. The coherent contributions result from the constructive interference of the light scattered by the atomic emitters, and provides the basis of optical cooperative effects [23–25]. These contributions include coherent backscattering and Mie scattering [26], and can be explained using a coherent dipole model [27, 28], or, in the case of cooperative scattering in the low-intensity regime, by the use of timed Dicke state approach [25]. The incoherent contribution is incoherent in a sense that the phase of the light scattered from different emitters

is random. This contribution includes diffuse scattering [26], and can be explained by the random walk model [27, 28]. Diffuse scattering induces the progressive attenuation of the laser intensity as it propagates through the cloud, which is called the shadow effect and can be explained by the Beer-Lambert law [26]. In addition, anisotropy of the emission pattern is observed, but this contribution is much smaller than the contribution of the shadow effect.

Over the past years, several experiments studied the radiation pressure force exerted by a cw laser on a cold atomic cloud [25, 28–30], to clarify the interplay between collective coherent and incoherent contributions to the radiation pressure force. Bienaime et al. [29] developed a cooperative radiation pressure force model based on the timed Dicke state approach and compared it with the experiment. Based on the results, they proposed to use the radiation pressure force as a new tool for the experimental investigation of cooperativity. This idea was extremely attractive and led to a series of new studies. Those studies, however, later indicated that specific effects observed in radiation pressure force may not always be a signature of cooperativity, i.e. coherent collective effects, but a result of different mechanisms associated with incoherent collective effects [26, 31].

In this paper we report on the role of collective effects on the FC-induced radiation pressure force acting on a cold cloud of ^{87}Rb atoms released from a magneto-optical trap (MOT). We have measured the FC force as a function of the comb mode detuning from the ^{87}Rb $|5S_{1/2}; F = 2\rangle \rightarrow |5P_{3/2}; F' = 3\rangle$ transition for different optical thicknesses of the atomic cloud. Reduction and broadening of the FC-induced force are observed as the cloud's optical thickness is increased. In order to understand the role of coherent and incoherent contributions to the FC-induced radiation pressure force, experimental results are compared to the predictions of the coherent timed Dicke state approach and an incoherent model

based on the Beer-Lambert law. Both models satisfactorily describe the experimental results, suggesting that the incoherent scattering approach is sufficient to explain the observed modifications of the FC force even in the case of larger optical thicknesses. Our results support the considerations in [26] for the case of cw-induced force and small optical thicknesses, thus verifying the analogy between FC and cw light-atom interactions.

The paper is organized as follows. In Sec. II we describe in detail the experimental setup, including the preparation of cold cloud of ^{87}Rb atoms of a given optical thickness and its determination, as well as the procedures for measuring the FC radiation pressure force. In Sec. IIIA, we present the measurements of the FC radiation pressure force as a function of comb detuning, and show that two distinct peaks appear in one f_{rep} scan, reflecting the interaction of three comb modes with three hyperfine transitions. The FC force is measured for different atom densities. In Sec. IIIB, we adopted the theoretical models developed in the literature for the case of cw radiation pressure force and applied them to calculate the FC-induced force. Given the very low intensity of the comb mode involved in the FC-atom interaction, we used a coherent model based on timed Dicke state approach and an incoherent model based on the Beer-Lambert law involving the shadow effect. In Sec. IIIC, we present the measured and calculated results of the reduction and broadening of the FC-induced force as a function of the cloud optical thickness, showing the agreement of both models with the measurements. We finish in Sec. IV with conclusion and outlook.

II. EXPERIMENT

A simplified scheme of the experimental setup for the preparation of a cold ^{87}Rb cloud and its characterization using absorption imaging, as well as the setup for FC radiation pressure force measurement using fluorescence imaging is shown in the Fig. 1(a).

Preparation of a cloud of cold atoms. A cold ^{87}Rb cloud is loaded from a background vapour in a stainless steel chamber using a standard six-beam configuration. The preparation of a cold ^{87}Rb cloud of a given optical thickness is achieved in three consecutive stages: MOT loading, temporal dark MOT, and repumping stage. In the first stage, we load the MOT for 6 s, with the cooling laser detuned -3.5Γ from the ^{87}Rb $|5S_{1/2}; F = 2\rangle \rightarrow |5P_{3/2}; F' = 3\rangle$ transition, and the repumper laser in resonance with the $|5S_{1/2}; F = 1\rangle \rightarrow |5P_{3/2}; F' = 2\rangle$ transition, generating a cloud of $\approx 4 \cdot 10^7$ atoms at a temperature of around $50 \mu\text{K}$, and a $1/e^2$ radius of ≈ 0.8 mm. Here $\Gamma = 6.07$ MHz is the natural linewidth of ^{87}Rb $|5S_{1/2}\rangle \rightarrow |5P_{3/2}\rangle$ hyperfine transition [32]. In the second stage, we apply a 15 ms long temporal dark MOT, where we reduce the power of the repumper laser to $10 \mu\text{W}$ and the detuning of the cooling laser to -2Γ . All other parameters remain unchanged. As a result, the

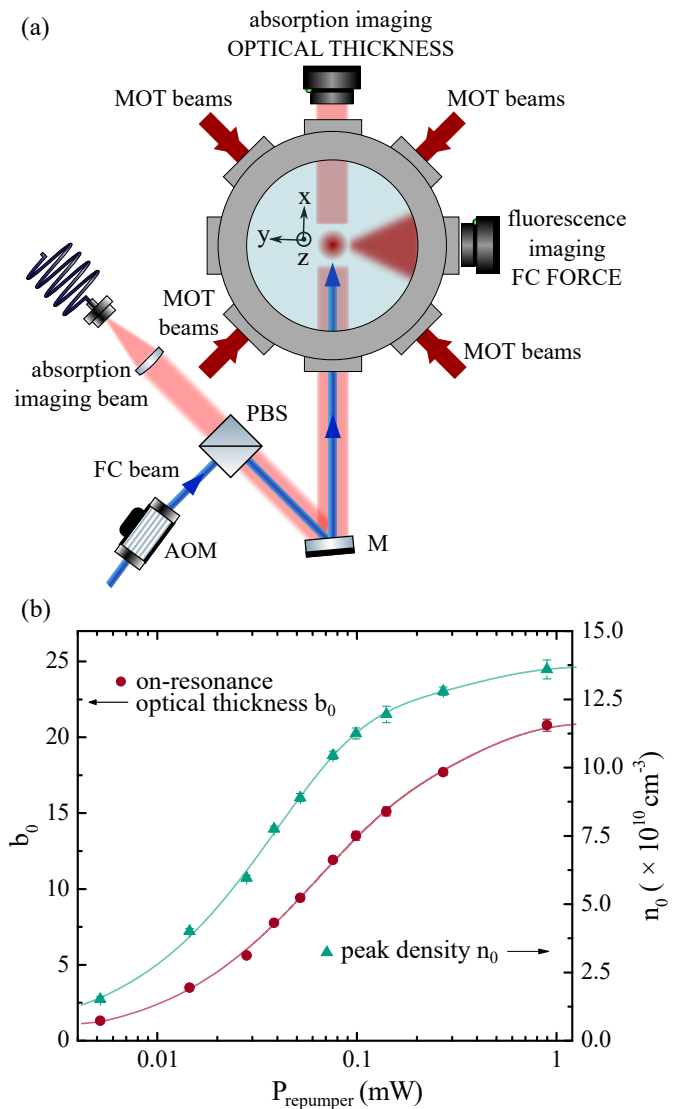


FIG. 1: (a) A simplified experimental scheme. Two pairs of counter-propagating MOT beams are shown, while the third pair is propagating in the z axis. The absorption imaging beam and the FC beam are co-propagated in the x -axis. The optical thickness is measured using the absorption imaging camera, while the FC force is measured using the fluorescence imaging camera. During the measurement of optical thickness, the FC beam is blocked using an AOM. M is a mirror and PBS is a polarizing cube. (b) On-resonance optical thickness (red circles) and cloud peak density (green triangles) as a function of the repumper laser power during the first, MOT loading stage. Solid lines represent a guide to the eye.

atoms are pumped into the $F = 1$ ground state, which causes an increase of the cloud density and, consequently, of the optical thickness. Finally, we increase the power of the repumper laser to 1.5 mW and tune the cooling laser to -7Γ , in order to re-cool and compress the cloud into a spherical shape in the repumping stage that lasts 1 ms. The power values given above correspond to the

total repumper power entering the vacuum chamber.

After preparing the cold cloud, we measure its optical thickness, $b(y, z)$, using the standard off-resonant absorption imaging technique. We image the spatial intensity distribution of a weak probe beam propagating in the x direction with no cloud present, $I_0(y, z)$, and with the beam passing through a ^{87}Rb cloud, $I(y, z)$, and calculate the optical thickness given by $b(y, z) = -\ln[I(y, z)/I_0(y, z)]$. For an atomic cloud of a Gaussian density distribution, $b(y, z)$ will also have a Gaussian shape. By fitting a 2D Gaussian to the measured $b(y, z)$, we extract the optical thickness at the centre of the cloud, b_{peak} , as well as R_y, R_z cloud radii. From b_{peak} we calculate the on-resonance optical thickness, b_0 , using $b_0 = b_{peak} \cdot (1 + 4\delta_{img}^2/\Gamma^2)$, where δ_{img} is the detuning of the probe laser frequency used for absorption imaging from the relevant atomic resonance frequency. In our case, the probe beam is 2.5 cm in diameter, has 30 μW of power and is 9.1 MHz red detuned from the $|5S_{1/2}; F = 2\rangle \rightarrow |5P_{3/2}; F' = 3\rangle$ transition, giving $b_0 = 10b_{peak}$. The imaging pulse duration is 50 μs . On-resonance optical thickness is defined as $b_0 = \sigma_0 \int_{-\infty}^{\infty} n(x, y=z=0) dx$, where σ_0 is on-resonance cross section [32], and $n(x, y, z) = n_0 \exp[-x^2/(2R_x^2) - y^2/(2R_y^2) - z^2/(2R_z^2)]$ is the Gaussian spatial density of the cloud with n_0 equal to peak density in its centre. The number of cold atoms in the cloud, N , and peak cloud density, n_0 , are then calculated from the measured optical thickness and radii using $N = (2\pi b_0 R_x R_y)/\sigma_0$ and $n_0 = 3N/(4\pi R_x R_y R_z)$.

In order to vary the optical thickness of the cloud, we change the power of the repumper laser in the first MOT loading stage, leaving the dark MOT and the repumping stage parameters unchanged. By changing the repumper power in the 5 μW - 1.5 mW range, the optical thickness measured for the $|5S_{1/2}; F = 2\rangle \rightarrow |5P_{3/2}; F' = 3\rangle$ transition can be varied from 1 to 21. However, changing the power of the repumper laser in the first stage also affects the other cloud parameters such as size, number of atoms, density, and temperature. Although a change in these parameters does not affect the accuracy of optical thickness determination since it is measured directly by absorption imaging, a detailed characterization of all cloud parameters is made as a function of the repumper laser in the first stage. In Fig. 1(b), the peak density and on-resonance optical thickness are shown as a function of the repumper laser power in the first, MOT loading stage. Both values initially increase linearly and saturate at higher repumper powers. The largest achieved on-resonance optical thickness is 21, the peak density is $1.3 \cdot 10^{11} \text{ cm}^{-3}$ which gives $n_0 k_0^{-3} = 2 \cdot 10^{-4}$, indicating a condition in which multiple scattering effects can be neglected [27, 31]. Here, $k_0 = 2\pi/(780 \text{ nm})$ is the wave vector relevant for the excitation of the ^{87}Rb $|5S_{1/2}\rangle \rightarrow |5P_{3/2}\rangle$ transition [32]. For the given range of repumper laser powers, the cloud temperature varies from 35 μK to 75 μK , where the temperature is measured using a standard time-of-flight (TOF) technique.

FC force measurement. The FC is generated by frequency doubling an Er: fiber mode-locked femtosecond laser (TOPTICA FFS) operating at 1560 nm with a repetition rate of $f_{rep} = 80.495 \text{ MHz}$. The frequency-doubled spectrum used in the experiment is centered around 780 nm with a FWHM of about 5 nm and a total output power of 76 mW. The FC spectrum consists of a series of sharp lines, i.e. comb modes [33]. The optical frequency of the n -th comb mode is given by $f_n = n \cdot f_{rep} + f_0$, where f_{rep} is the laser repetition rate and f_0 is the offset frequency. In our experiment, we actively stabilize f_{rep} and f_n by giving feedback to the cavity length and pump power of the mode-locked laser, thus indirectly fixing f_0 . The detuning of the n -th comb mode with respect to the $|5S_{1/2}; F = 2\rangle \rightarrow |5P_{3/2}; F' = 3\rangle$ transition is varied by scanning f_0 while keeping f_{rep} fixed. A detailed description of the FC stabilization and scanning scheme is presented in our recent papers [11, 12].

After the cold cloud is prepared, it is illuminated by the FC beam, exerting a FC-induced radiation pressure force on the cloud's centre of mass (CM). The force is measured as a function of the detuning of the n -th comb mode with respect to the $|5S_{1/2}; F = 2\rangle \rightarrow |5P_{3/2}; F' = 3\rangle$ transition. The experimental setup and the measurement sequence used are similar to the ones described in our recent works [11, 12]. A linearly polarized FC beam is sent through an acousto-optic modulator (AOM) for fast switching, and is directed to the center of the cloud. The total power of the FC beam on the atoms is 25 mW and the beam size (FWHM) is 2.7 mm, resulting in the power and intensity per comb mode of about 0.75 μW and 9 $\mu\text{W}/\text{cm}^2$, respectively. The measurement sequence starts with the preparation of a cloud of a given optical thickness. At $t = 0$ we turn off the MOT cooling beams and switch on the FC beam. The MOT repumper lasers are left on continuously to optically pump the atoms out of the $|5S_{1/2}; F = 1\rangle$ ground level. They are arranged in a counter-propagating configuration with the intensity predominantly in the direction perpendicular to the FC beam propagation, and have no measurable mechanical effect. The quadrupole magnetic field is also left on. We let the comb interact with the cold cloud for 0.5 ms. During this time the center of mass of the cloud accelerates in the FC beam direction ($+x$ -direction) due to the FC radiation pressure force. The FC beam and repumper lasers are then switched off, and the cloud expands freely for a variable time t_{free} , after which we switch on the MOT cooling beams for 0.15 ms and image the cloud's fluorescence with a camera. The times t_{free} are chosen to maximize both the CM displacement and the signal-to-noise ratio and are varied from 4 ms (for the smallest b_0) to 18 ms (for the largest b_0). This measurement sequence is repeated 3 times for each detuning of the FC mode from the $|5S_{1/2}; F = 2\rangle \rightarrow |5P_{3/2}; F' = 3\rangle$ transition, and the resulting fluorescence images are averaged. The cloud's CM displacement in the $+x$ -direction is determined from the images, providing information on the cloud's acceleration and the FC radiation pressure force.

We then change the optical thickness of the cloud and repeat the measurement sequence.

It is worth noting here that the approaches to changing the optical thickness of the cloud by changing the repumper laser power immediately after dark MOT stage used in [29], and by changing the cloud's free expansion time used in [19] are not applicable in our case of the FC excitation. In the first approach, only a fraction of atoms are transferred from $|5S_{1/2}; F=1\rangle$ to $|5S_{1/2}; F=2\rangle$ ground level after the dark MOT, depending on the repumper laser power. Atoms remaining in the $|5S_{1/2}; F=1\rangle$ level and atoms in $|5S_{1/2}; F=2\rangle$ could be simultaneously excited by different comb modes, which would result in a complex lineshape of the measured FC force. In the second approach, the size of the FC beam should be at least twice the initial size of the cloud, which cannot be achieved in our setup due to the low power per comb mode.

III. RESULTS AND DISCUSSION

A. FC force as a function of cloud density

In Fig. 2(a) we show the measured FC force as a function of the FC detuning δ , which we define as the detuning of the n -th comb mode from the $|5S_{1/2}; F=2\rangle \rightarrow |5P_{3/2}; F'=3\rangle$ transition, for different peak cloud densities, n_0 . Due to the nature of the comb spectrum, the FC radiation pressure force is periodic with respect to the comb detuning with period equal to f_{rep} . Two distinct peaks appear in one f_{rep} scan reflecting the interaction with three comb modes, as explained in detail in our recent work [11]. The peak at $\delta = 0$ is due to the n -th comb mode being in resonance with the $|5S_{1/2}; F=2\rangle \rightarrow |5P_{3/2}; F'=3\rangle$ transition, whereas the peak at $\delta \approx -25.5$ MHz is due to the $(n-3)$ -rd mode being in resonance with the $|5S_{1/2}; F=2\rangle \rightarrow |5P_{3/2}; F'=2\rangle$ transition, and the $(n-5)$ -th mode in resonance with the $|5S_{1/2}; F=2\rangle \rightarrow |5P_{3/2}; F'=1\rangle$ transition. For completeness, in Fig. 2(b) we show the calculated FC force, obtained by summing the contributions from three hyperfine transitions (for details on FC force calculations see [11]).

As the cloud density increases, reduction and broadening of both FC force peaks is observed. In addition, the ratio of the peaks at $\delta = 0$ and $\delta \approx -25.5$ MHz decreases with increasing the cloud density, as can be seen from the inset in the Fig. 2(a). The peak ratio of 2.8 is expected when n_0 approaches zero, as it reflects the ratio of the $|5S_{1/2}; F=2\rangle \rightarrow |5P_{3/2}; F'=3\rangle$ and $|5S_{1/2}; F=2\rangle \rightarrow |5P_{3/2}; F'=2\rangle$ transition dipole matrix elements [32]. This behaviour can be easily understood, given the well-known finding that collective effects such as force reduction and broadening depend on the optical thickness rather than the density [27]. The observed dependence of the peak ratio on the cloud density is the result of the different optical thicknesses of the two peaks

for a given optical density. As the optical thickness is defined through the cross section $\sigma_0 = h\omega\Gamma/(2I_{\text{sat}})$, where I_{sat} is the saturation intensity depending on the dipole moment of the relevant transition [32], the two peaks have different optical thicknesses for a given density and therefore different factors of force reduction, which directly affects the peak ratio. In the following sections we will therefore present and analyze the dependence of the FC force on the optical thickness for each force peak separately.

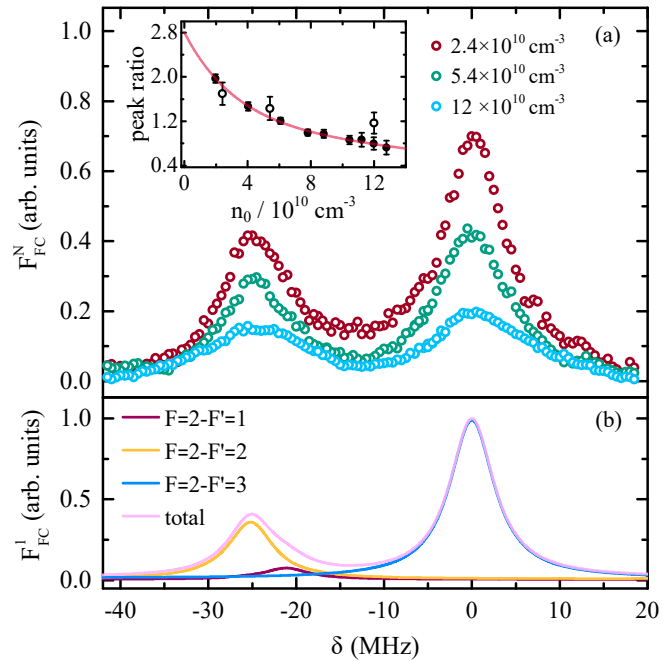


FIG. 2: (a) Measured FC force as a function of the FC detuning δ , for different peak atom densities n_0 . The inset shows the ratio of the FC peak forces at $\delta = 0$ and $\delta \approx -25.5$ MHz where the symbols are experimental data and the line represents a guide to the eye. Full circles correspond to averaged multiple scans, as described in the experimental section. Empty circles correspond to peak ratios of the scans shown in (a), which were taken without averaging and thus have larger errors. (b) Calculated FC force as a function of the FC detuning δ . The total FC force (violet line) is obtained by summing the force contributions from three $|5S_{1/2}; F=2\rangle \rightarrow |5P_{3/2}; F'=1, 2, 3\rangle$ hyperfine transitions.

B. Theoretical models

In this work we use an analytical expression for the cw cooperative radiation force in the presence of disorder developed in [29], based on the timed Dicke state, as well as the results of an incoherent model based on the Beer-Lambert law to calculate the FC force. We compare both theoretical approaches with experimental results and draw a conclusion about the role of incoherent and coherent scattering in the FC radiation pressure

force. In doing so, we imply that only a single comb mode (the one closest to resonance) dominates the light-atom interaction, i.e. the effects associated with other comb modes can be neglected since they are detuned from the atomic resonances [11, 12]. In this respect we can consider a single comb mode participating in the interaction as a cw laser.

The radiation pressure force acting on the j -th atom, \hat{F}_j , can be derived from the laser-atom interaction Hamiltonian describing the excitation of N two-level atoms with a cw laser beam propagating in \hat{z} direction, giving:

$$\hat{F}_j = \hat{F}_{aj} + \hat{F}_{ej}, \quad (1)$$

where \hat{F}_{aj} is the force contribution associated with absorption of photons from the laser beam and \hat{F}_{ej} is the force contribution arising from emission of photons in arbitrary directions. The average radiation pressure force defined as $\hat{F} = (1/N) \sum_j \hat{F}_j = (F_{tot}/N)\hat{z}$ accelerates the cloud's CM in the direction of beam propagation, with the acceleration given by $\hat{a}_{CM} = \hat{F}/m$ where m is the single atom mass. A detailed derivation of the average cw radiation pressure force resulting from the excitation of N atoms by a resonant laser can be found in [34], and is given by:

$$F = \frac{hk_0\Gamma}{4\pi N} \int_0^{2\pi} d\phi \int_0^\pi d\theta \sin\theta (1 - \cos\theta) I_s(\theta, \phi). \quad (2)$$

$I_s(\theta, \phi)$ is the scattered far-field intensity given by $I_s(\theta, \phi) = \sum_{j=1}^N |\beta_j|^2 + \sum_{j \neq m=1}^N (\beta_j \beta_m^* \exp[-i\mathbf{k} \cdot (\mathbf{r}_j - \mathbf{r}_m)])$, where the angles θ, ϕ determine the direction of the emitted photon with the wave vector \mathbf{k} , and β_j and \mathbf{r}_j are the atomic coherence and position of the j -th atom, respectively. Equation (2) shows that the radiation pressure force that accelerates the atoms along the direction of the incident laser beam is proportional to the net radiation flux of the scattered intensity, i.e. the pattern of the scattered intensity is directly mapped to the radiation pressure force. In addition, it should be noted that the force has two contributions: one incoherent that is proportional to excitation probability of individual atomic dipoles $\sum_{j=1}^N |\beta_j|^2$, and the other coherent due to the interference between the different atomic dipoles.

In the case of incoherent scattering, the second term in $I_s(\theta, \phi)$ is equal to zero, and the light is scattered isotropically. I_s can be calculated from the transmitted intensity governed by the Beer-Lambert law, i.e. $I_s = I_0 [1 - \exp(-b(x, y))]$, where I_0 is the intensity of the incident laser beam. $b(x, y) = b_0 / (1 + 4\delta^2/\Gamma^2) \cdot \exp[-x^2/(2R_x^2) - y^2/(2R_y^2)]$, with b_0 equal to on-resonance optical thickness and δ to the detuning of the incident laser frequency from the atomic resonance frequency. Due to the Beer-Lambert law, the laser intensity attenuates as it propagates through the cloud, and the radiation force decreases accordingly. This effect is called the shadow effect. The radiation pressure force in the presence of the shadow effect is derived from

Eq. (2) in [26], and is given by:

$$\frac{F_{shadow}}{F_1} = \frac{\text{Ein}(b)}{b}, \quad (3)$$

where $\text{Ein}(b)$ is the entire function given by $\text{Ein}(z) = \int_0^z dx (1 - e^{-x})/x$, with $b = b_0 / (1 + 4\delta^2/\Gamma^2)$, and F_1 the single-atom radiation pressure force. F_1 has a Lorentzian shape and for small intensities of the incident laser, $I_0/I_{sat} \ll 1$, is given by $F_1 = \sigma_0 I_0 / [ck^2 (1 + 4\delta^2/\Gamma^2)]$.

The inclusion of coherent effects in the force calculations requires the second term in $I_s(\theta, \phi)$. A convenient model to calculate this full, many-body problem is to use the coupled dipole model and to expand the atomic coherences β_j for n -th order scattering events [26, 27, 35, 36]. This approach is beyond the scope of this work. Instead, a mean-field approach inspired by the timed Dicke state model is used. This model assumes that all atoms are driven by the unperturbed laser beam, i.e. the atoms acquire the phase of the laser and all have the same excitation probabilities characterized by $\beta_j = \beta/\sqrt{N} \cdot \exp(i\mathbf{k}_0 \cdot \mathbf{r}_j)$. Timed Dicke state approach has become widely used in recent years, as it gives a description of experimental results on superradiance, subradiance and frequency shifts that are observed in light scattered by cold atomic ensembles. Such emission is called cooperative because it is the result of cooperative activity of many coherent atomic dipoles [24], and the radiation pressure force that results from such an emission is called cooperative radiation force. cw cooperative radiation force is studied in detail in [29, 30]. The average force, F_{coop} , can be estimated by:

$$\frac{F_{coop}}{F_1} = \frac{4\delta^2 + \Gamma^2}{4\delta^2 + (1 + b_0/12)^2\Gamma^2} \left[1 + \frac{b_0}{24(k_0 R)^2} \right], \quad (4)$$

where $R^2 = R_x^2 + R_y^2 + R_z^2$ is the cloud radius, and F_1 is the single atom force given above. The model neglects reabsorption of photons by other atoms, and is usually used in the limit of small intensities or large detunings.

In this work we apply equations (3) and (4) to our experimental parameters, and calculate the average radiation pressure force on the CM of a cold ^{87}Rb cloud in the presence of shadow (i.e. incoherent collective), and cooperative (i.e. coherent collective) effects and compare it to the measured FC force induced by a single FC comb mode.

C. Collective effects in the FC force

In Fig. 3 we show the measured FC force as a function of the FC detuning δ , for different on-resonance optical thicknesses b_0 , in the case of $|5S_{1/2}; F = 2\rangle \rightarrow |5P_{3/2}; F' = 2, 3\rangle$ excitations. In the case of the $|5S_{1/2}; F = 2\rangle \rightarrow |5P_{3/2}; F' = 3\rangle$ transition, b_0 is measured directly as described in Sec. II, and divided by 2.8 to obtain b_0 relevant for the $|5S_{1/2}; F = 2\rangle \rightarrow |5P_{3/2}; F' = 2\rangle$ transition. The same figure also shows

the cooperative radiation pressure force calculated for our experimental parameters using Eq. (4), where δ is the detuning of the n -th comb mode from the $|5S_{1/2}; F = 2\rangle \rightarrow |5P_{3/2}; F' = 3\rangle$ transition, $\Gamma = 6.07$ MHz, $k_0 = 2\pi/(780$ nm), $R=0.3$ mm and b_0 corresponds to the measured values.

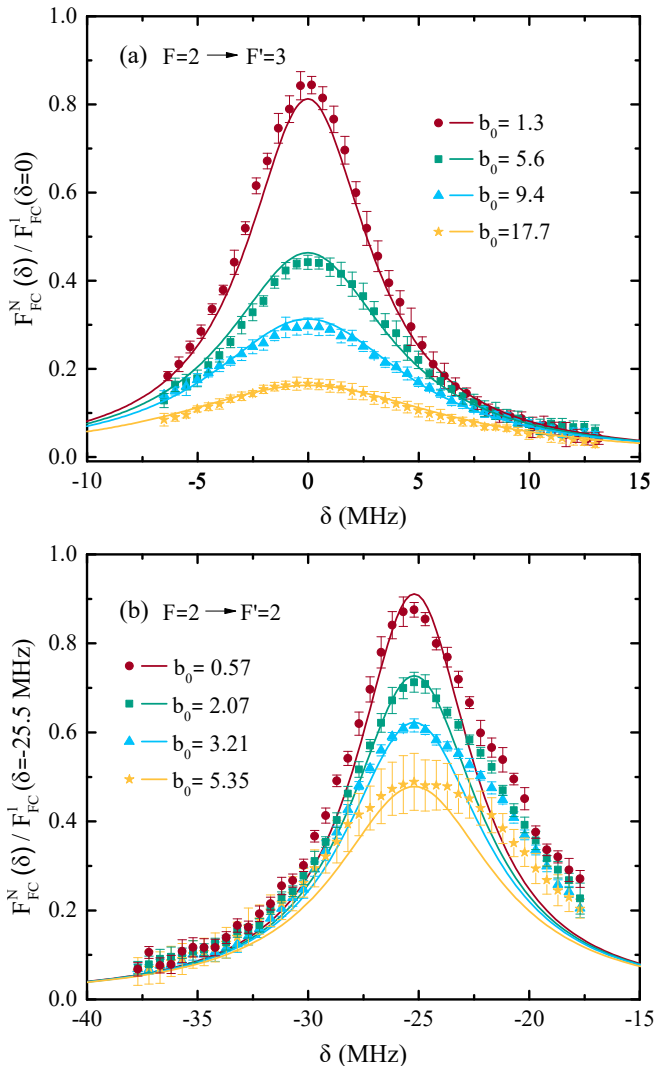


FIG. 3: Measured FC force (symbols) and cooperative radiation pressure force calculated using Eq. (4) (lines) as a function of δ , for different optical thicknesses b_0 . (a) FC force is due to the n -th comb mode being in resonance with the $|5S_{1/2}; F = 2\rangle \rightarrow |5P_{3/2}; F' = 3\rangle$ transition. (b) FC force is due to the $(n - 3)$ -rd mode being in resonance with the $|5S_{1/2}; F = 2\rangle \rightarrow |5P_{3/2}; F' = 2\rangle$ transition.

The measured FC forces arising from the $|5S_{1/2}; F = 2\rangle \rightarrow |5P_{3/2}; F' = 3\rangle$ transition show a Lorentzian line shape in the whole range of measured b_0 , for $0.5 \leq b_0 \leq 20.8$, Fig. 3(a). In the case of the $|5S_{1/2}; F = 2\rangle \rightarrow |5P_{3/2}; F' = 2\rangle$ transition, the FC forces deviate from the Lorentzian line shape, Fig. 3(b), due to the $|5S_{1/2}; F = 2\rangle \rightarrow |5P_{3/2}; F' = 1\rangle$ FC force contribution positioned in the blue wing of the peak, as indicated in the Fig. 2(b).

For a given b_0 , the Lorentzian function is fitted to the experimental data to obtain the FC force line center, linewidth, peak value, and offset. While the FC force offset should be zero, experimentally we see a small offset due to inaccuracies in determination of the initial and final position of the cloud's CM, from which the acceleration, i.e. the force is determined. The small FC force offset is subtracted from all experimental data shown in the Figs. 3 and 4.

The FC force reduction and broadening is clearly observed for both peaks shown in Figs. 3(a) and 3(b) and presented in more details in Fig. 4. The reduction is defined as $F_{FC}^N(\delta)/F_{FC}^1(\delta)$, and shown in Fig. 4(a) for $\delta = 0$ and $\delta = -\Gamma$ in the case of $|5S_{1/2}; F = 2\rangle \rightarrow |5P_{3/2}; F' = 3\rangle$ transition, and for $\delta = -25.5$ MHz and $\delta = -25.5$ MHz $-\Gamma$ in the case of $|5S_{1/2}; F = 2\rangle \rightarrow |5P_{3/2}; F' = 2\rangle$ transition. In order to obtain $F_{FC}^1(\delta)$ and to normalize our data, the measured FC force values as a function of b_0 for a given detuning δ , $F_{FC}^N(\delta)$, are fitted with the Eq. 4 with $F_{FC}^1(\delta)$ as a free fitting parameter. Thus determined $F_{FC}^1(\delta)$ is then used as a scaling factor for normalization of the FC forces shown in Figs. 2, 3 and 4(a).

In Fig. 4(a) we show the measured FC force reduction along with the predictions of theoretical models discussed above, i.e. shadow and cooperative effects, calculated using Eqs. (3) and (4), respectively. We observe a reduction of the FC force with increasing b_0 . The FC force reduction is larger when the relevant comb mode is resonant with a given atomic transition, i.e. the n -th comb mode in resonance with the $|5S_{1/2}; F = 2\rangle \rightarrow |5P_{3/2}; F' = 3\rangle$ transition ($\delta = 0$), and the $(n - 3)$ -rd mode being in resonance with the $|5S_{1/2}; F = 2\rangle \rightarrow |5P_{3/2}; F' = 2\rangle$ transition ($\delta = -25.5$ MHz). Both models give similar theoretical predictions for the force reduction with increasing b_0 and support the experimental results.

In Fig. 4(b) we show the measured FC force linewidths Γ_{FC} as a function of b_0 along with predictions of the discussed theoretical models of shadow and cooperative effects, calculated using Eqs. (3) and (4), respectively. For a given b_0 , Γ_{FC} is obtained from the fit of a Lorentzian function to the FC force experimental data. We observe the increase of the FC linewidth with increasing b_0 . At $b_0 = 0$, the FC linewidth of $\Gamma = 6.07$ MHz is expected, as it reflects the natural linewidth of the ^{87}Rb $|5S_{1/2}\rangle \rightarrow |5P_{3/2}\rangle$ transition [32]. For the largest $b_0 = 20.8$ achieved in the experiment, the FC force linewidth of 2.5Γ is measured. The force linewidth in the presence of cooperative effects calculated using Eq. (4) shows a linear increase with increasing b_0 (violet solid line in Fig. 4(b)) as this model does not include multiple scattering effects that can induce the flattening of the force linewidth curve at large b_0 [30]. The force linewidth in the presence of the shadow effect calculated using Eq. (3) recovers the linear dependence of the force linewidth for small b_0 and predicts a nonlinear dependence of the linewidth for a large b_0 (green dashed line in Fig. 4(b)). Although for the measured range of b_0 the difference in

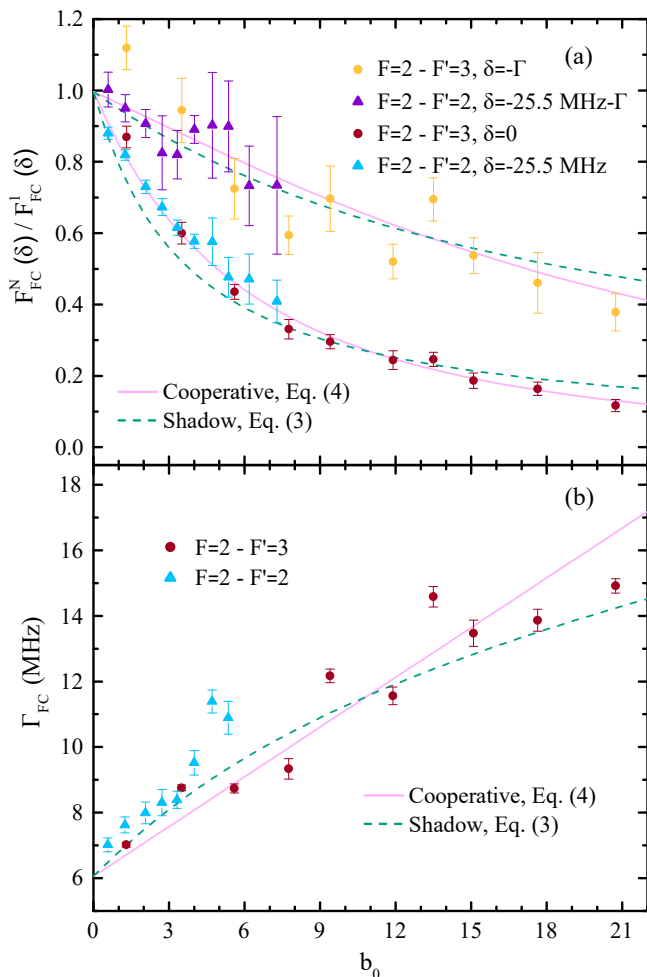


FIG. 4: Signature of collective effects in the FC force arising from the ^{87}Rb $|5S_{1/2}; F=2\rangle \rightarrow |5P_{3/2}; F'=2\rangle$ and ^{87}Rb $|5S_{1/2}; F=2\rangle \rightarrow |5P_{3/2}; F'=3\rangle$ transitions. (a) Measured FC force reduction (symbols) and calculated force reduction in the presence of shadow (dash line) and cooperative (solid line) effects, using Eq. (3) and (4), respectively, as a function of b_0 for $\delta=0$ and $\delta=-\Gamma$ in the case of $|5S_{1/2}; F=2\rangle \rightarrow |5P_{3/2}; F'=3\rangle$ transition, and $\delta=-25.5 \text{ MHz}$ and $\delta=-25.5 \text{ MHz}-\Gamma$ in the case of $|5S_{1/2}; F=2\rangle \rightarrow |5P_{3/2}; F'=2\rangle$ transition. (b) Measured FC force broadening (symbols) and calculated force broadening in the presence of shadow (green dashed line) and cooperative (violet solid line) effects, using Eq. (3) and (4), respectively, as a function of b_0 .

the force linewidths predicted by these two models is not significant, in Fig. 4(b) there are indications that the shadow effect model more accurately supports our experimental results.

IV. CONCLUSION

In conclusion, we have measured the frequency-comb-induced radiation pressure force acting on a cold ^{87}Rb

cloud in the presence of collective effects which depend on the cloud's optical thickness. We observed reduction and broadening of the frequency comb force as the optical thickness increases. Theoretical models for cw radiation pressure force in the presence of shadow and cooperative effects developed in [26] and [29], respectively, are used to describe the measured frequency comb force. Both theoretical models support the experimental results well, thus verifying the analogy between the comb and cw atom-light interaction, which is in line with previous investigations of the comb-induced force on atoms [11, 12]. In addition, showing a good agreement of both timed Dicke state and shadow effect models with measured comb-induced force, we have extended the validity of the conclusions presented in [26] even for larger optical thicknesses.

Our results show that the influence of off-resonance comb modes on the comb-atom interaction is minor and can be neglected, even in the case of increased optical thickness of the cloud. In addition, our results indicate that the observed frequency comb force reduction and broadening arise as a result of the shadow effect describing the progressive attenuation of the light intensity in the cloud due to the Beer-Lambert law and that it is therefore not necessary to use numerically more demanding coherent atom-light interaction models to describe the observed effects. The results presented in this paper contribute to the understanding of scattering of frequency comb light by an ensemble of cold atoms, which pave the way toward novel frequency comb applications in the field of cooling and trapping, quantum communication, and light-atom interfaces based on structured and disordered atomic systems.

V. ACKNOWLEDGEMENT

The authors acknowledge support from the Croatian Science Foundation (Project Frequency comb cooling of atoms - IP-2018-01-9047). The authors acknowledge Neven Šantić for reading the manuscript and providing constructive comments, as well as for his early contribution to the development of cold atoms experiment. In addition, the authors acknowledge Ivor Krešić for the early contribution to the development of theoretical models as well as Grzegorz Kowzan and Piotr Masłowski for their contribution to the frequency comb stabilization.

- [1] J. Ye, H. Schnatz, and L. W. Hollberg, *IEEE J. Sel. Top. Quantum Electron* **45**, 1041–1058 (1998), URL <https://ieeexplore.ieee.org/document/1250461>.
- [2] T. Rosenband et al., *Science* **319**, 1808–1812 (2008), URL <https://science.sciencemag.org/content/319/5871/1808>.
- [3] S. A. Diddams, L. Hollberg, and V. Mbele, *Nature* **445**, 627–630 (2007), URL <https://doi.org/10.1038/s41566-018-0347-5>.
- [4] P. Maslowski, K. Cossel, A. Foltynowicz, and J. Ye, *Cavity-Enhanced Spectroscopy and Sensing* (Springer, Berlin, 2014), URL <https://link.springer.com/book/10.1007/978-3-642-40003-2>.
- [5] N. Picque and T. Hänsch, *Nature Photonics* **13**, 146–157 (2019), URL <https://doi.org/10.1038/s41566-018-0347-5>.
- [6] K. Minoshima and H. Matsumoto, *Appl. Opt.* **39**, 5512–5517 (2000), URL <https://www.osapublishing.org/ao/abstract.cfm?URI=ao-39-30-5512>.
- [7] M. T. Murphy et al., *Monthly Notices of the Royal Astronomical Society* **380**, 839–847 (2007), URL <https://academic.oup.com/mnras/article/380/2/839/1016250>.
- [8] J. Davila-Rodriguez, A. Ozawa, T. W. Hänsch, and U. T., *Phys. Rev. Lett.* **116**, 043002 (2016), URL <https://doi.org/10.1103/PhysRevLett.116.043002>.
- [9] M. Ip, A. Ransford, A. M. Jayich, X. Long, C. Roman, and W. C. Campbell, *Phys. Rev. Lett.* **121**, 043201 (2018), URL <https://journals.aps.org/prl/abstract/10.1103/PhysRevLett.121.043201>.
- [10] A. M. Jayich, X. Long, and W. C. Campbell, *Phys. Rev. X* **6**, 041004 (2016), URL <https://doi.org/10.1103/PhysRevX.6.041004>.
- [11] N. Šantić, D. Buhin, D. Kovačić, I. Krešić, D. Aumiler, and T. Ban, *Sci Rep* **6**, 2510 (2019), URL <https://doi.org/10.1038/s41598-018-38319-3>.
- [12] D. Buhin, D. Kovačić, F. Schmid, M. Kruljac, V. Vulić, T. Ban, and D. Aumiler, *Phys. Rev. A* **102**, 021101(R) (2020), URL <https://doi.org/10.1103/PhysRevA.102.021101>.
- [13] Y. Cai, J. Roslund, G. Ferrini, F. Arzani, X. Xu, C. Fabre, and N. Treps, *Nat Commun* **8**, 15645 (2017), URL <https://www.nature.com/articles/ncomms15645>.
- [14] M. Kues, C. Reimer, P. Roztocky, et al., *Nature* **546**, 622–626 (2017), URL <https://www.nature.com/articles/nature22986>.
- [15] C. Reimer et al., *Science* **351**, 1176–1180 (2016), URL <https://science.sciencemag.org/content/351/6278/1176/tab-article-info>.
- [16] G. Maltese, M. I. Amanti, F. Appas, et al., *npj Quantum Inf.* **6**, 13 (2020), URL <https://doi.org/10.1038/s41534-019-0237-9>.
- [17] I. Krešić, M. Kruljac, T. Ban, and D. Aumiler, *JOSA B* **36**, 1758–1764 (2019), URL <https://www.osapublishing.org/josab/fulltext.cfm?uri=josab-36-7-1758&id=413602>.
- [18] D. Main, T. M. Hird, S. Gao, I. A. Walmsley, and P. M. Ledingham (2020), 2011.03765.
- [19] S. Bromley, B. Zhu, M. Bishof, et al., *Nat Commun* **7**, 11039 (2016), URL <https://www.nature.com/articles/ncomms11039>.
- [20] J. Pellegrino, R. Bourgain, S. Jennewein, Y. Sortais, A. Browaeys, S. Jenkins, and J. Ruostekoski, *Phys. Rev. Lett* **113**, 133602 (2014), URL <https://journals.aps.org/prl/abstract/10.1103/PhysRevLett.113.133602>.
- [21] S. D. Jenkins, J. Ruostekoski, J. Javanainen, S. Jennewein, R. Bourgain, J. Pellegrino, Y. R. P. Sortais, and A. Browaeys, *PRA* **94**, 023842 (2016), URL <https://doi.org/10.1103/PhysRevA.94.023842>.
- [22] S. Balik, A. L. Win, M. D. Havey, I. M. Sokolov, and D. V. Kupriyanov, *PRA* **87**, 053817 (2013), URL <https://doi.org/10.1103/PhysRevA.87.053817>.
- [23] J. Rui, D. Wei, A. Rubio-Abadal, S. Hollerith, J. Zeiher, D. M. Stamper-Kurn, C. Gross, and I. Bloch, *Nature* **583**, 369 (2020), URL <https://doi.org/10.1038/s41586-020-2463-x>.
- [24] R. H. Dicke, *Phys. Rev.* **93**, 99 (1954), URL <https://journals.aps.org/pr/abstract/10.1103/PhysRev.93.99>.
- [25] S. Bux et al., *Journal of Modern Optics* **57**, 1841–1848 (2010), URL <https://doi.org/10.1080/09500340.2010.503011>.
- [26] R. Bachelard, N. Piovella, W. Guerin, and R. Kaiser, *Phys. Rev. A* **94**, 033836 (2016), URL <https://doi.org/10.1103/PhysRevA.94.033836>.
- [27] B. Zhu, J. Cooper, J. Ye, and A. M. Rey, *Phys. Rev. A* **94**, 023612 (2016), URL <https://journals.aps.org/pr/abstract/10.1103/PhysRevA.94.023612>.
- [28] J. Chabé, M. Rouabah, L. Bellando, T. Bienaimé, N. Piovella, R. Bachelard, and R. Kaiser, *Phys. Rev. A* **89**, 043833 (2014), URL <https://doi.org/10.1103/PhysRevA.89.043833>.
- [29] T. Bienaimé, S. Bux, E. Lucioni, P. Courteill, N. Piovella, and K. R., *Phys. Rev. Lett* **104**, 183602 (2010), URL <https://journals.aps.org/prl/abstract/10.1103/PhysRevLett.104.183602>.
- [30] P. W. Courteille, S. Bux, E. Lucioni, K. Lauber, T. Bienaimé, R. Kaiser, and N. Piovella, *Eur. Phys. J. D* **58**, 69–73 (2010), URL <https://doi.org/10.1140/epjd/e2010-00095-6>.
- [31] W. Guerin, M. O. Araújo, and R. Kaiser, *Phys. Rev. Lett.* **116**, 083601 (2016), URL <https://doi.org/10.1103/PhysRevLett.116.083601>.
- [32] D. A. Steck, Rubidium 87 D Line Data (revision 2.2.1, 2019), URL <http://steck.us/alkalidata/rubidium87numbers.pdf>.
- [33] S. T. Cundiff and J. Ye, *Femtosecond Optical Frequency Comb: Principle, Operation and Applications* (Springer, Berlin, 2005), URL <http://www.springer.com/us/book/9780387237909>.
- [34] T. Bienaimé, R. Bachelard, J. Chabé, M. Rouabah, L. Bellando, P. W. Courteille, N. Piovella, and R. Kaiser, *Journal of Modern Optics* **61**, 18–24 (2014), URL <https://doi.org/10.1080/09500340.2013.829264>.
- [35] T. Bienaimé, M. Petruzzo, D. Bigerni, N. Piovella, and R. Kaiser, *Journal of Modern Optics* **58**, 1942–1950 (2011), URL <https://doi.org/10.1080/09500340.2011.594911>.
- [36] J. Javanainen, J. Ruostekoski, B. Vestergaard, and M. R. Francis, *Phys. Rev. A* **59**, 649 (1999), URL <https://doi.org/10.1103/PhysRevA.59.649>.